# Synthetic aperture focusing techniques for ultrasonic imaging of solid objects.

Tadeusz Stepinski
Uppsala University, Sweden

Fredrik Lingvall
NORSAR, Kjeller, Norway

## Abstract

Synthetic aperture focusing technique (SAFT) has been used in non-destructive testing mainly in its simplest form that mimics acoustic lenses used for focusing ultrasonic beams at a point of a solid object or structure. This paper presents a review of SAFT algorithms applied for post-processing of ultrasonic data acquired in non-destructive inspection of metals. The performance of SAFT in terms of its spatial resolution and suppression of the backscattering from material structure is discussed. The discussion is illustrated by the experimental data obtained from the ultrasonic inspection of test specimens with artificial defects (side drilled holes).

## 1 Introduction

Synthetic aperture focusing techniques (SAFT) aim at improving the lateral resolution of ultrasound images by extending aperture of a physical source achieved by processing several successive measurements. SAFT has been used in ultrasonic imaging systems mainly due to its two benefits: first, it improves the lateral resolution in a broad focal zone, and second, it is capable of improving contrast in ultrasonic images by reducing backscattering effects due to the coarse material structure.

Usually, the NDE and medical SAFT implementations are performed using a delay-and-sum (DAS) processing in time-domain [1]. DAS is a straightforward way of mimicking lens effect, which is commonly used in phased arrays. Frequency-domain implementations of SAFT that have been widely used for many years in radar (synthetic aperture radar, SAR) and sonar (synthetic aperture sonar, SAS), are still relatively unknown in NDE and medical applications.

Most SAFT implementations are based on a very simplified model of the imaging system used for developing radar and sonar applications. Such implementations can perform relatively well provided that the theoretical assumptions, generally valid for SAR and SAS, are fulfilled in the particular application. The principal assumption, which is usually correct in radar and sonar, is that the region of interest (ROI) is located in the far field of the transducer (antenna) used for creating synthetic array, where its specific diffraction effects can be neglected (point-like source assumption). Unfortunately, this is not always valid in ultrasonic imaging, especially in the high frequency NDE applications where the transducer is often in contact with the inspected structure.

At least two kinds of problems may be encountered in such setup, firstly, transducer's diffraction effects may impair image quality, and secondly, sparse spatial sampling used for gathering ultrasonic data may yield aliasing artifacts in the resulting image.

## 2 Time Domain SAFT Imaging

There are two setups that are normally used in NDE for ultrasonic inspection of solid objects: contact and immersion mode. In contact mode ultrasonic transducer is directly coupled to the surface of the inspected object using a thin layer of contact agent. In the immersion mode object and transducer are immersed in a liquid medium (commonly water) and ultrasonic waves propagate towards the inspected object through a thick water layer.

### 2.1 Contact Mode SAFT

The immersion setup can be represented by the simplified SAFT system model presented in Fig. 1, [2].

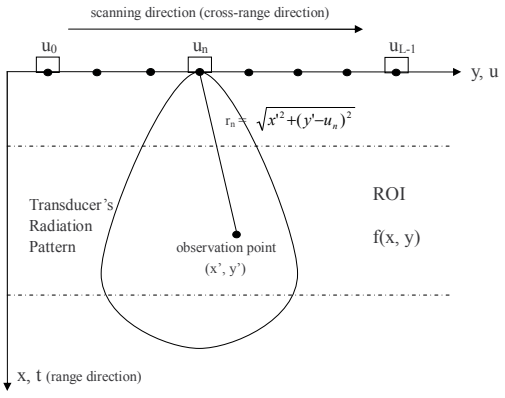


**Figure 1:** 2D geometry representing SAFT in contact mode. Ultrasonic transducer is shifted in discrete steps along the scanning direction.

It is assumed that the stationary target region in the spatial $(x, y)$ domain contains a number of omni-directional and frequency independent reflecting targets. Transducer moves along the $u$ axis, which is parallel to the $y$ axis of the target area, and transmits a wide bandwidth phase modulated waveform $p(t)$.

To achieve focus at an observation point $(x', y')$ in the ROI, the SAFT system performs a coherent summation of the time-shifted received signals $s(t, x_n)$ measured at transducer positions $x_n$ for all $n$ in the synthetic aperture.

The time delays, $\tau_n$, aiming to compensate for different times of flight, can be expressed as $\tau_n = \frac{2}{c}(r_n - x') = \frac{2}{c}(\sqrt{x'^2 + (y' - u_n)^2} - x')$ for $n = 0, 1, ..., L-1$, where $L$ is the number of element positions, $r_n$ is the distance from the element at a position $u_n$ to the observation point. Weight coefficients (apodization) $a_n$ are often used to control the sidelobe levels.

## 2.2 Immersion Mode SAFT

In the immersion mode a reliable acoustic coupling is provided by immersing a test object in a tank filled with liquid. The ultrasonic transducer is placed under water and moved by a mechanical scanner to scan a ROI in the object. For the immersion mode, the ultrasonic waves propagate in two different media (water and solid) and the acoustic path between the transducer and the target is no longer a straight line. The difference between acoustic impedance of water and the impedance of inspected material, such as steel, results in refraction at the interface. According to the Fermat's principle the ultrasonic waves propagate between two points along the path which takes the least time.

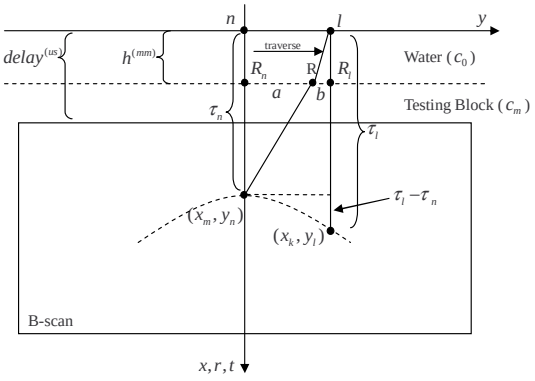


**Figure 2:** Propagating ultrasonic waves in immersion mode. *B-scan* indicates limits of the ROI within the solid test block.

As shown in Fig. 2, transducer beam is refracted at the point $R$ between $R_n$ and $R_l$ at the boundary between water and solid. To determine the time delay $\tau_l$ for each transducer position $(0, y_l)$ and each point within the ROI $(x_m, y_n)$ the position of $R$ has to be known (i.e., $a$ and $b$ are to be known). The refraction point $R$ can be determined either using Snell's low or Fermat's principle. Using Snell's law leads to a nonlinear equation, solution of which may be time consuming. A simple search scheme for all candidate points between $R_l$ and $R_n$ yields the point $R$ with least propagation time according to the Fermat's principle. The search is to be repeated for all points $(x_m, y_n)$ in the ROI and all transducer positions $(0, y_l)$. When the refraction points and the velocities $c_0$ and $c_m$ are known the respective delays $\tau_{lmn}$ can be calculated using geometrical relations.

## 2.3 Experimental Results

A series of experiments was performed to verify the performance of the SAFT algorithms in terms of resolution and suppression of the backscattering from material structure. Here, we present selected results obtained in contact mode for a cast austenitic steel cube #90646 from the Swedish nuclear power plant, shown in Fig.3 (details can be found in [2]).

Three side drilled holes (SDHs) with different diameters located at the depth of approx. 40 mm under the cube's upper surface were used as targets, as shown in Fig.3. Contact transducer from Panametrics with diameter 0.5 inch and center frequency 2.25 MHz was used for the inspection.

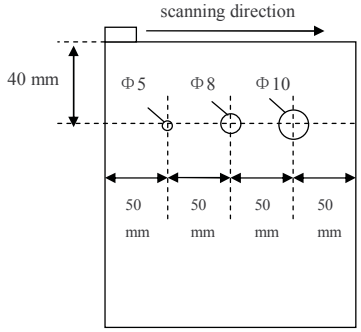


**Figure 3:** Austenitic steel block used in the experiment.

The original B-scan data and the SAFT result are plotted in Fig. 4 and the respective *profile* plots (max amplitude in each A-scan plotted vs the scanning distance) are shown in Fig. 5. It can be seen that the resolution of the raw B-scan is quite poor and a high level of material noise due to the backscattering from the coarse steel structure is observed. After SAFT processing, the resolution is considerably improved and the noise level due to the backscattering is considerably reduced. Note, that the holes have relatively large diameter, which has an apparent effect on the time of flight at the B-scan responses; the response of the largest hole (the right one) appears at the shorter range than that of the smallest one.

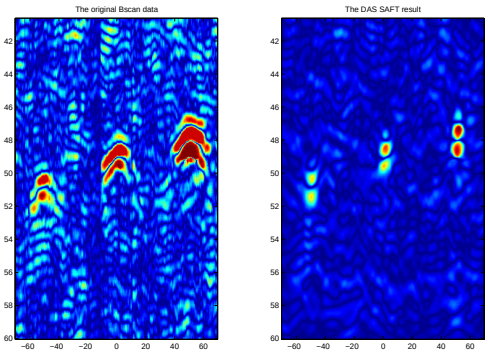


**Figure 4:** B-scans acquired in the experiment: raw data (left) and SAFT processed data (right).

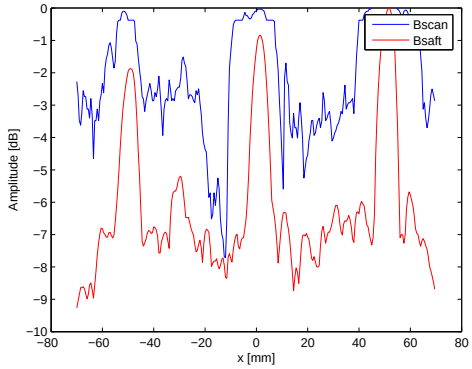


**Figure 5:** Cross-range profiles showing the maximum width of the hole responses calculated for the B-scans presented in Fig. 4.

# 3 Model Based High Resolution Synthetic Aperture Imaging

Here, we outline the method based on a discrete linear model of the imaging system proposed by Lingvall *et al* [3, 4]. The method uses a spatio-temporal deconvolution technique designed to minimize the mean squared reconstruction error of the imaging system. The transducer diffraction effects and electro-acoustical properties of the transducer introduce a position dependent smearing which results in an unsharp ultrasonic image. To improve resolution in the ultrasonic images a linear model of the imaging system is used and then a linear filter is applied that minimizes the mean squared error (MMSE) of the imaging system.

Now, consider scattering from point-like targets. The electrical output $s_{\mathrm{o}}(y,t)$ of an ultrasonic imaging system operating in pulse-echo mode can then be modeled as a sum of convolutions where the sum is taken over all point targets at the positions defined by $\mathcal{T}$. The output can be expressed as

$$s_{\mathrm{o}}(y,t) \propto \sum_{(y_{\mathrm{T}},x_{\mathrm{T}})\in\mathcal{T}} h_c^{\mathrm{SIR}}(y-y_{\mathrm{T}},x_{\mathrm{T}},t)* \\ h_{\mathrm{e}}(t) * s_{\mathrm{i}}(t) + e(t) \tag{1}$$

where $h_c^{\mathrm{SIR}}$ is the double path continuous time spatial impulse response (SIR), $h_{\mathrm{e}}(t)$ is the double path electrical impulse response, $e(t)$ is the measurement noise, and $s_{\mathrm{i}}(t)$ is the excitation signal.

A time-discrete version of (1) is obtained by sampling the SIRs and the electrical impulse response, and replacing the continuous time convolutions by their discrete time equivalents. A discrete representation of the targets is obtained by defining the so called *object function* $o(y,x)$, and let the discrete version of $o(y,x)$ be represented by the $M \times N$ matrix $\mathbf{O}$. Now, let $(y_{\tilde{n}}, x_m)$ denote the (discrete) observation point and $y_n$ the transducer position. A discrete version of (1) for an A-scan measurement vector can then be expressed as

$$\mathbf{z}_n = \sum_{\tilde{n}=n-L}^{n+L} \mathbf{P}_{d(\tilde{n},n)}\mathbf{o}_{\tilde{n}} + \mathbf{e}_n \tag{2}$$

where $\mathbf{e}_n$ is an additive noise, and $\mathbf{P}_{d(\tilde{n},n)}$ is a matrix consisting of finite impulse responses defined by the discrete impulse responses $\mathbf{h}_{d(\tilde{n},n)} \triangleq \mathbf{h}^{\mathrm{SIR}}_{d(\tilde{n},n)} * \mathbf{h}_e * \mathbf{s}_i$, for $\tilde{n} = n-L \ldots n+L$. That is, the vector $\mathbf{o}_{\tilde{n}}$ denotes the $\tilde{n}$th column in $\mathbf{O}$, and the matrix $\mathbf{P}_{d(\tilde{n},n)}$ contains the sampled, double-path, impulse responses at a distance $d(\tilde{n},n) = y_{\tilde{n}} - y_n$ (which is the horizontal distance between the observation point and the transducer, see Fig. 1). Eq. (2) is a discrete time model for a single A-scan measurement.

By vectorizing $\mathbf{O}$ and the B-scan measurement matrix into column vectors $\mathbf{o}$ and $\mathbf{y}$ respectively, a B-scan model can be expressed according to

$$\mathbf{z} = \mathbf{P}\mathbf{o} + \mathbf{e} \tag{3}$$

where $\mathbf{P}$ is a matrix consisting of impulse responses for all transducer positions and all observation points. Eq. (3) is a discrete linear model for ultrasonic imaging where the backscattering is considered as a sum of responses from point targets.

## 3.1 The Reconstruction Filter

The reconstruction filter is found by minimizing the mean squared reconstruction error

$$\begin{aligned} J &= E\{\|\mathbf{o}-\mathbf{K}\mathbf{z}\|^2\} \\ &= \mathrm{tr}\{\mathbf{C}_{\mathrm{o}}\} - 2\mathrm{tr}\{\mathbf{K}\mathbf{P}\mathbf{C}_{\mathrm{o}}\}+ \\ &\quad \mathrm{tr}\{\mathbf{K}(\mathbf{P}\mathbf{C}_{\mathrm{o}}\mathbf{P}^T + \mathbf{C}_{\mathrm{e}})\mathbf{K}^T\} \end{aligned} \tag{4}$$

where $\mathrm{tr}\{\cdot\}$ is the trace operator, $E\{\cdot\}$ the expectation operator, and $\mathbf{C}_{\mathrm{e}}$ and $\mathbf{C}_{\mathrm{o}}$ are the covariance matrices of the noise $\mathbf{e}$ and the object function $\mathbf{o}$, respectively.

The filter matrix, $\hat{\mathbf{K}}$, which minimizes (4), is the minimum mean square error estimator for the linear model (3) [3]

$$\begin{aligned}\hat{\mathbf{K}} &= \arg\min_{\mathbf{K}} J \\ &= \mathbf{C}_\mathrm{o}\mathbf{P}^T(\mathbf{P}\mathbf{C}_\mathrm{o}\mathbf{P}^T + \mathbf{C}_\mathrm{e})^{-1} \\ &= (\mathbf{C}_\mathrm{o}^{-1} + \mathbf{P}^T\mathbf{C}_\mathrm{e}^{-1}\mathbf{P})^{-1}\mathbf{P}^T\mathbf{C}_\mathrm{e}^{-1}.\end{aligned} \tag{5}$$

An estimate of the object function $\hat{\mathbf{o}}$, which is a filter with the minimum mean squared error for the imaging system, can now be obtained by performing the matrix-vector multiplication $\hat{\mathbf{K}}\mathbf{z}$ or by solving the equation system $(\mathbf{C}_\mathrm{o}^{-1} + \mathbf{P}^T\mathbf{C}_\mathrm{e}^{-1}\mathbf{P})\hat{\mathbf{o}} = \mathbf{P}^T\mathbf{C}_\mathrm{e}^{-1}\mathbf{z}$.
Note that although there are no assumptions regarding the shape of the transducer's active area nor the form of its electrical impulse response these parameters will be vital in the total performance of the imaging system.

### 3.2 Experimental Results

The performance of the MMSE algorithm and the time-domain SAFT algorithm was compared experimentally for imaging an immersed copper block shown in Fig. 6.
The measurements where performed using a phase array (PA) system that facilitates the measurements since the transmitting aperture easily can be changed by selecting the different numbers of active elements. In our experiments all active elements were fired simultaneously to simulate a planar (non-focused) transducer.

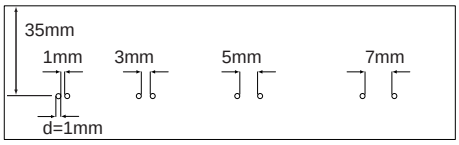


**Figure 6:** Copper test block with twin side-drilled holes.

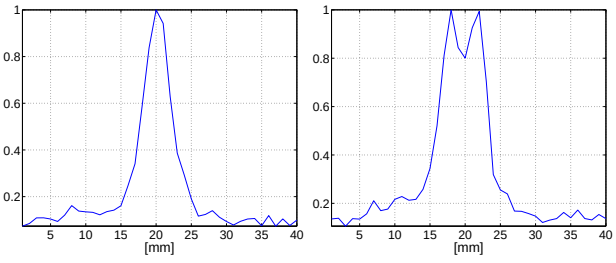


**Figure 7:** Profile plots of the SAFT processed data acquired with a 1 mm transducer. $\Delta d$ = 1 mm (left) and 5 mm (right).

The B-scan data were recorded with a spatial sampling distance of 1 mm between the individual A-scans. The synthetic aperture for the MMSE and the SAFT algorithms was 31 mm. The SIRs used for the MMSE method where computed using an analytic solution for a line-strip transducer that where sampled and adapted to the immersed solid case using Snell's law. The selected results are shown as profile plots in Fig. 7 and 8. The distance $\Delta d$ denotes the spacing between the SDHs.

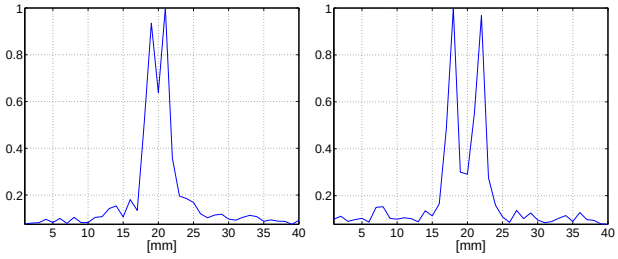


**Figure 8:** Profile plots of the MMSE processed data acquired with a 1 mm transducer. $\Delta d$ = 1 mm (left) and 5 mm (right).

The results from the MMSE method (see Fig. 8) show that the MMSE method yields better resolution than ordinary SAFT. The SAFT was able to resolve the SDHs with spacings of $\Delta d \geq 5$ mm while the MMSE resolved the SDHs with $\Delta d \geq 1$ mm. From the experiments performed using a large aperture could be seen that the performance of the SAFT method deteriorates when the transducer size increases.

## 4 Conclusions

SAFT processing is an effective tool improving spatial resolution and contrast in ultrasonic images.
Transducer diffraction effects can be compensated using the model based MMSE algorithm for postprocessing ultrasonic data.

## References

[1] Schmitz, V.; Chakhlov, S.; Müller, W.: *Experiences with synthetic aperture focusing in the field*, Ultrasonics, Vol. 38, 2000, pp. 731–38.

[2] Stepinski, T.: *SAFT Performance in ultrasonic inspection of coarse grained metals*, Proc. of the 6th Int. Conf. on NDE in Relation to Structural Integrity for Nuclear Pressurised Components, Budapest, 8–10 October, 2007.

[3] Lingvall, F.; Olofsson, T.; Stepinski, T.: *Synthetic aperture imaging using sources with finite aperture: Deconvolution of the spatial impulse response*, J. Acoust. Soc. Amer., vol. 114, no. 1, July 2003, pp. 225–34.

[4] Lingvall, F.; Olofsson, T.: *On Time-domain Model Based Ultrasonic Array Imaging*, IEEE Trans. on Ultrasonics, Ferroelectrics, and Frequency Control, vol 54, no 8, 2007, Aug. 2007, pp. 1623-1633.